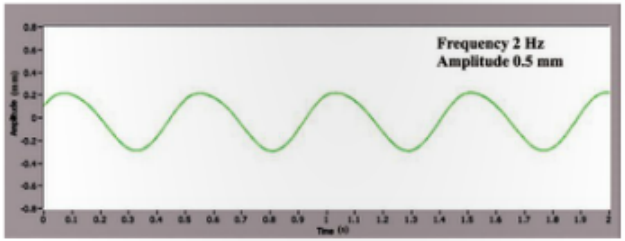

Fig. 7 : LVDT reference signal

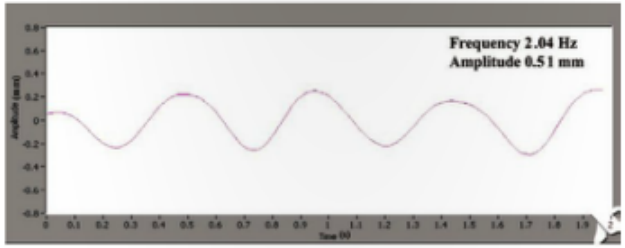

Fig. 8 : Vibration signal extracted from the ultrasonic A-scan signals

whose imaginary part is the Hilbert Transform of original time signal.

$$z(t) = x(t) + jy(t) = E(t)e^{j\Psi(t)} \qquad (2)$$

Where, E(t) is the instantaneous envelope which is the magnitude of the complex analytic signal, and Ψ(t) is the phase angle of analytic signal. Fig.6 shows the envelope extraction of a typical ultrasonic A-scan signal acquired during subassembly vibration at frequency of 2 Hz and amplitude of 0.5 mm (pk-pk). After envelope extraction, the time difference (transit time) between the peak value of transmitted pulse and received echo is found. As the velocity of ultrasound in water is known, the displacement of target (subassembly) is calculated from the transit time. When subassembly vibrates, displacement of target changes and hence transit time changes. The transit time is calculated for all the ultrasonic A-scan signals and the displacement signal is generated. Fig.7 shows the vibration (displacement) signal extracted from the ultrasonic signals and Fig.8 shows the reference signal recorded from the LVDT for an excitation frequency of 2 Hz and amplitude 0.5 mm (pk-pk). The amplitude and frequency of vibration of subassembly measured using ultrasonic technique were 0.51 mm (pk-pk) and 2.04 Hz respectively. This vibration signal is matching well with the reference signal from LVDT. The signals from the ultrasonic sensor and the reference LVDT sensor were analyzed for various subassembly excitation frequencies and amplitudes, and the overall error in this measurement technique is found to be less than 3 %.

5. CONCLUSION

Ultrasonic technique and its signal processing algorithm have been developed for the subassembly vibration measurements in PFBR. Experiments were carried out in a water test loop using a PFBR full scale dummy fuel subassembly. Amplitude and frequency of vibration of fuel subassembly measured using ultrasonic technique is compared with a reference LVDT sensor and the error was found to be less than 3%. The developed technique proved to be a potential and promising NDE method for vibration measurement, where the conventional contact type sensors cannot be used.

REFERENCES

1. V. Prakash et.al, Experimental qualification of subassembly design for Prototype Fast Breeder Reactor, Nuclear Engineering and Design, Vol. 241, No.8, pp.3325– 3332, August 2011.

2. R.Ramakrishna et.al, Flow Induced Vibration measurement using Ultrasonic Technique, International Conference on Sensors & Related Networks (SENNET 2009), VIT, Vellore, India, Dec 07-10, 2009.

3. M. Anandaraj et.al, Flow induced vibration studies on PFBR fuel subassembly, 2nd International Conference on Asian Nuclear Prospects, ANUP 2010, Chennai, India, Oct 10-13, 2010.

On the conversion of multi-frequency "apparent" conductivity data to actual conductivity gradients on peened samples

Veeraraghavan Sundararaghavan[1] and Krishnan Balasubramaniam[2]
Center for Non-Destructive Evaluation, Machine Design Section, Department of Mechanical Engineering,
Indian Institute of Technology-Madras, Chennai 600036, India.
[2] E-mail: balas@iitm.ac.in
[1] Currently with Department of Aerospace Engineering, University of Michigan, Ann Arbor, MI, USA

ABSTRACT

This paper addresses the interpretation of "apparent" conductivity measurements as a function of frequency in order to determine the actual conductivity profile as a function of depth in a conducting material. Simulations show that "apparent" conductivities are not indicative of actual conductivity gradients because of inherent constant conductivity approximation that is assumed at every frequency. This paper focuses on facilitating the conversion of the multi-frequency "apparent" conductivity data conductivity depth profiles through a Model based inversion scheme. The inversion uses a multi-layer axi-symmetric finite element model as the forward model and uses an optimal skin depth approximation for isolating the integral effects of the conductivity gradients on the multi-frequency "apparent" conductivity measurements. Unlike the inductance inversion method that has been reported elsewhere, this method does not depend on the sensor coil parameters and is robust enough to accommodate for some common measurement uncertainties. Also, commercial multi-frequency conductivity measurement instruments can be used to obtain input data for the inverse model. Possible application of the model towards characterization of residual stresses in peened specimens is also addressed.

Keywords: Multi-Frequency Eddy Current Testing; Inverse Model; Conductivity Gradient Measurements

1. INTRODUCTION

Eddy current NDT techniques are well developed and have been primarily applied as a means of detecting near surface discontinuities. The changing voltage in the sensor coil induces eddy currents in a nearby conductor that in turn loads the coil and changes its impedance and phase. The depth of penetration of eddy currents can be controlled by the frequency of testing, due to the skin-depth effect, and hence, can be used to test components over different depths. Eddy current testing methodology has been successfully applied over the years to address problems like crack detection, material thickness measurements, heat damage detection, "apparent" conductivity measurements and for monitoring a variety of processes (ASNT (2004)). A method for assessing "apparent" conductivity involves measurement of the impedance of coils, driven by a constant amplitude alternating current, placed above the sample surface. Material is assumed to have a constant conductivity and the net conductivity is measured at various frequencies using eddy current absolute-coil configuration (ASTM E 1004-99).

A conductivity measurement at a particular frequency has information from the surface to a particular depth of penetration that is related to the skin-depth (d) in that material. Also, it represents an integrated value of conductivity over this depth. Hence, when making measurements of "apparent" conductivity at different frequencies, these measurements are not independent of each other, since any measurement at a lower frequency has the information already existing in all of the measurements made using higher frequencies.

Any NDE process may be considered to involve three systems, each having a unique set of parameters that define its characteristics viz. (a) The Input to the material, (b) The material itself, and (c) The output response measured by the NDE system. Traditionally, the input and the material parameters are assumed known and numerous Forward Models have been developed that predict or estimate the output response function. Over the years, forward models are very well established and serve the key purpose, for improved interpretation as well as to optimize the input parameters to obtain the desired output response. The other two scenarios i.e. if the output response function in the form of measured data is available, to obtain one of system parameters, i.e. either the input function or the material properties while the other one is assumed to be known are classified as Inverse Problems. Due to the availability of computational resources, the inverse problem solutions are becoming increasingly feasible. The traditional difficulties with the ill-posedness of the inverse solution (which includes lack of uniqueness or stability of the solution process) are increasingly becoming solvable. Typical applications include measurement of material properties such as modulus, viscosity, temperature, hardness and stress profiles, etc. The formulation includes both numerical and analytical solutions in ultrasonics, eddy current and thermal imaging

and the inverse solution process utilizes a variety of techniques such as Neural Networks, Genetic Algorithms, Maximum Entropy Methods, etc (Liu, 2003).

Popular methods to invert eddy current impedance data include the use of regressive tools like neural networks or numerical inversion schemes based on analytical or finite element based forward models. The use of neural networks for conductivity inversion has been reported by several authors (Rekanos et al., 1997; Katragadda et al., 1997; Glorieux et al., 1999) with inverse models being trained using either experimental data or data from numerical models. The proposed "apparent" conductivity inversion scheme is primarily a numerical inversion scheme based on a Finite element based forward model. Seminal work on numerical inversion of multi-frequency eddy current impedance measurements for characterizing coating thicknesses and conductivities in layered materials can be found in Moulder et al. 1992. More advanced numerical inversion models (Bowler and Norton, 1993; Liu et al., 2000; Sun et al., 2002 etc.) primarily work by iteratively adjusting relevant parameters in a forward model until measured signal value is reached. Such techniques require accurate calibration of coil design parameters for use in the forward model. The proposed "apparent" conductivity inversion model is different from other existing numerical models in that it does not employ any form of iterative refinement and further, does not depend on coil design parameters, hence, can be used with commercial conductivity meters.

"Apparent" conductivity measurements using the eddy current sensor have been widely used as a basis for characterizing surface-treated specimens. This work was motivated by a study of finite element simulations that showed that the "apparent" conductivity does not follow the trends followed by the actual conductivity profiles. Specifically, an attempt is made here to study the effect of peening on true conductivity profiles of a specimen using the proposed inversion scheme. Studies have been performed (Blodgett et al., 2003; Lavrentyev et al., 2000) to analyze the effect of peening on a material using change of measured "apparent" conductivity with frequency. The conductivity of the peened specimen continuously changes as a function of depth due to interacting effects of several factors including cold work gradients, surface roughness, and stress gradients. However, "apparent" conductivity profiles are only able to provide a depth-averaged response

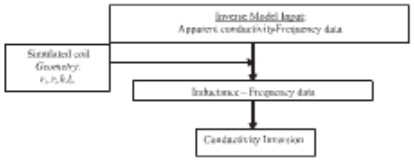

Fig. 1 : Proposed "apparent" conductivity inversion procedure

of a peened specimen. Hence, there is a need for an appropriate inversion scheme that can recover the information-rich actual conductivity profiles from such measurements. This paper extends the inductance inversion technique already proposed (Sundararaghavan and Balasubramaniam, 2004; Sundararaghavan et al. 2005) to invert multi-frequency "apparent" conductivity data measured over nonmagnetic metals. The true conductivity profiles show several promising trends that would possibly allow characterization of residual stresses in peened specimens.

2. METHODOLOGY OF INVERSION

The critical input for the inversion model comes in the form of "apparent" conductivity measurements at various frequencies. The "apparent" conductivity measurement is based on the notion that the material has a single conductivity that contributes to the measured inductance of the coil placed over the material. Given the "apparent" conductivity, the expected inductance change of any coil placed over the material can be found using existing eddy current forward models which are either analytical (Dodd et al., 1970) or based on the Finite element method. In this paper, finite element forward model (FEFM) (Palanisamy, 1980) is used to estimate the inductance values of a simulated coil placed over the material with the given "apparent" conductivity at a particular excitation frequency. For applications involving conductivity variation with depth in axi-symmetric testing situations, apart from Finite element based models, numerical models such as those reported by Uzal et al. (1993) can also be used as the forward model. The proposed "apparent" conductivity processing procedure is depicted in Figure 1. Finite element technique using the energy functional approach (Palanisamy, 1980) is used to solve the axi-symmetric eddy current governing equation for the magnetic vector potentials (A) in the discretized domain consisting of coil, material and air (Figure 2). The governing equation for axisymmetric geometries is given by,

$$\frac{1}{\mu}\left(\frac{\partial^2 A}{\partial r^2}+\frac{1}{r}\frac{\partial A}{\partial r}+\frac{\partial^2 A}{\partial z^2}-\frac{A}{r^2}\right)=-J_s+\sigma\frac{\partial A}{\partial t} \qquad (1)$$

Given the "apparent" conductivity (σ_a) of the material at frequency, f, the current density (J_s) in the coil and known geometrical parameters (r_o,r_i,h,l_o,d) as shown in Figure 2, the magnetic vector potentials (A) can be calculated over all nodes in the discretized domain. Only nonmagnetic materials are considered, hence we use the permeability of free space, μ_0. The impedance (Z_{coil}) of the coil whose cross section is discretized into N triangular finite elements is then calculated as,

$$Z_{coil}=\frac{2\pi j\omega N_s}{I_s}\sum_{j=1}^{N} r_{cj}A_j\Delta_j \qquad (2)$$

where j is the complex operator, N_s is the turn density of the coil (turns/m^2), I_s is the current in the coil, ω is the

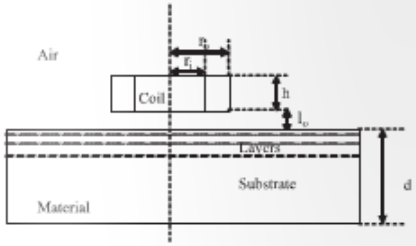

Fig. 2 : Finite element model configuration

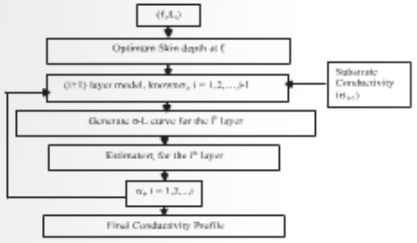

Fig. 3 : Multi-frequency inductance inversion scheme

angular frequency of the excitation current, and r_{cj}, A_{cj}, Δ_{cj} are the centroidal radius, centroidal magnetic vector potential and the area of the jth triangular element in the finite element mesh respectively. The FEFM was verified by comparing the results with the analytical model reported by Dodd and Deeds (1968). The self-inductance (L_{ii}) of a coil, whose height, outer radius, inner radius and number of turns are 6.35 mm, 9.525 mm, 3.175 mm, and 200 respectively, was calculated using both techniques. Analytical solution yields a self-inductance of 3.217x10^{-4} Henries while the FEFM solution gives a self-inductance of 3.216 x 10^{-4} Henries, a net error less than 0.1 %. Based on these results, the confidence in the FEFM for axi-symmetric cases was established.

Once the measured "apparent" conductivities are converted to inductance values of a simulated coil, a multi-frequency inductance inversion model (Sundararaghavan and Balasubramaniam, 2004; Sundararaghavan, et al., 2005) is used to obtain the conductivity profiles. The conductivity profile is assumed to be discontinuous, piecewise constant and each constant conductivity layer is modeled by several rows of triangular elements. The multi-frequency inductance data inversion scheme is depicted in Figure 3. During the inductance inversion process, frequencies are first sorted in the descending order. The highest frequency, corresponding to the least depth of penetration according to the optimal skin depth approximation, is used in the first solution step of the inverse model. Since the substrate conductivity is known, a two-layer model (optimal skin depth at the highest frequency and the substrate) can be used to separate the conductivity of the topmost layer. During this step, the finite element forward model assigns a range of conductivity values to the topmost layer and calculates the inductance of the coil. The actual inductance value is then matched to a particular value of conductivity by rational interpolation of the conductivity-inductance data.

In the subsequent step of the inversion scheme, a lower coil excitation frequency is used as the input to the inverse model. In this case, the depth of penetration is higher than that of the first frequency input, and the eddy current penetrates the top layer whose conductivity was already found during the first step. A three-layer model with this top layer, a second layer of unknown conductivity and the substrate can be used to find the unknown conductivity by following a procedure similar to the first solution step of the inversion process. In the nth step, an n+1-layered model is used. The inversion method generates the depth-conductivity profile within "n" steps. This technique can be applied for measurements peened samples on which the stresses are inherently axi-symmetric (Sundararaghavan et al. (2005)).

Since the inverse model uses the apparent conductivity data directly, only test specimen related parameters like base conductivity and material thickness need to be provided to the inverse model. The measurement is performed at each frequency at two levels as discussed before, (1) Experimental measurement of "apparent" conductivity using a conductivity meter and (2) a computer simulated measurement of inductance of a simulated coil over the material using the set up shown in Figure. 2. In the simulated measurement, the virtual test specimen is given a uniform conductivity corresponding to the effective conductivity of the specimen as measured by the conductivity meter in step (1). The second step employs a simulated air-core coil whose parameters are given in Table. 1. This is an advantage over the multi frequency inductance inversion scheme where customized coils were fabricated and the coil parameters and lift off have to be measured accurately and fed into the inverse model (Sundararaghavan et al., 2005). Since the proposed model works with apparent conductivities as an input, the inductance measurement is performed on computer using the Finite element model.

3. MODEL VALIDATION

The forward model is used to generate the "apparent" conductivity inputs for the inversion model given any conductivity profile. The methodology for the forward problem is shown in Figure 4. Piecewise constant conductivity profiles were simulated on the material with a conductivity of 28 MS/m and a relative permeability of 1 assigned to the substrate for all simulations. The FEFM is used to measure the inductance of a coil placed over the material with the known conductivity profile. The geometrical parameters of the simulated coil used for the simulations are specified in Table-1. A conductivity-

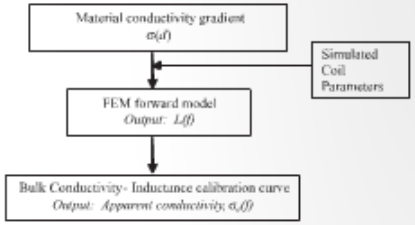

Fig. 4 : Forward Problem: Obtaining "apparent" conductivity from the conductivity profile

inductance calibration curve is used to calculate the "apparent" conductivities corresponding to the measured inductances at various frequencies. The calibration curve for any particular measurement configuration can be generated using the finite element forward model.

Two different piecewise continuous conductivity profiles were simulated on the material and are plotted in Figure 5. The "apparent" conductivities at 6 different frequencies for each of these profiles are shown alongside the simulated profiles. The "apparent" conductivity-frequency data was inverted using the proposed algorithm using an optimum skin depth of 2d.

Table – 1 : Properties of the simulated pancake coil

Property	*Value*
Number of Turns	240
Outer radius (r_o mm)	4.3
Inner radius (r_i mm)	2.5
Lift Off (l_o mm)	4
Thickness (h mm)	15

A comparison of the actual conductivity profile and the "apparent" conductivity measurements in Figure 5 reveals that the trends in "apparent" conductivity are not indicative of the actual conductivity gradients in the material. For example in Figure 5(a), the actual conductivity gradient is monotonically increasing whereas the "apparent" conductivity plot in Figure 5(b) does not show any such trend. It must also be noted here that for a monotonic change in actual conductivity of about 25%, the corresponding change in the "apparent" conductivity is of the order of only about 1%. Also, the "apparent" conductivity measurements are significantly influenced by the top most layer conductivity. Similarly, for case in Figure 5b, a 10% change in actual conductivity brings about changes in the "apparent" conductivity of the order of only 1%. This FEFM result clearly shows the reason for the lack of sensitivity of the "apparent" conductivity measurement to conductivity depth profiling during

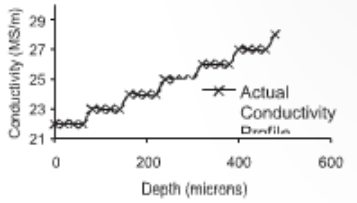

(a) Profile-1: Monotonically Increasing conductivity

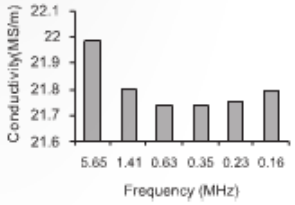

(b) "apparent" Conductivity for Profile1

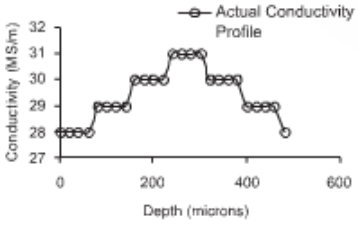

(c) Profile-2: Increasing and decreasing conductivity

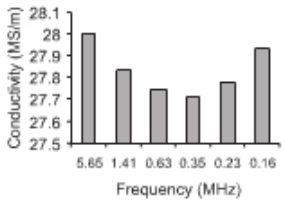

(d) "apparent" Conductivities for Profile2

Fig. 5 : Simulated conductivity profiles and "apparent" conductivity measurements at 6 different frequencies

measurements of material properties such as stress as reported elsewhere (Lavrentyev et al., 2000; Blodgett et. al. (2003)).

The "apparent" conductivity data was then used an input into the inversion model and the reconstructed actual conductivity profiles are compared with the input actual conductivity profiles in Figure 6. The "apparent" conductivity inversion methodology was implemented using C++ solvers for the eddy current forward FEM problem and a LabVIEW graphical user interface. The method is computationally efficient and consumes 0.1 seconds for each "apparent" conductivity measurement on a 2.2 GHz Pentium IV PC. Hence, the methodology has scope for applicability in online monitoring where the profiles are expected to be axisymmetric, in processes such as peening and heat treatment.

An analysis of Figure 6 indicates that the correlation between the actual conductivity and the reconstructed conductivity is excellent near the surface, but the reconstruction error progressively increases with depth. The increase in reconstruction error with depth can be attributed to the skin depth approximation used in the proposed incremental layer approach. The skin depth (d) in the proposed model was calculated based on the substrate conductivity since the actual conductivities are not known prior to the reconstruction. Future work might involve optimization of the skin depths based on an iterative framework using an initial guess based on the substrate conductivity for the reconstruction. It must also be noted that substrate conductivity is not easily obtained. These may be coarsely approximated by the "apparent" conductivity measured over surface unaltered specimens at low frequencies or by using the intrinsic volumetric conductivity of the material.

4. SENSITIVITY OF "APPARENT" CONDUCTIVITY BASED INVERSION

It is difficult to quantify the error in the multi-frequency inductance inversion scheme since the procedure is dependant on accurate measurement of multiple coil geometry parameters. There is a need for an inversion procedure that works regardless of the measurement sensor design. In the "apparent" conductivity inversion technique, the only eddy current measurement input is the "apparent" conductivity. These values can be measured using several available commercial conductivity meters within an accuracy of +0.5% IACS by calibrating against reference

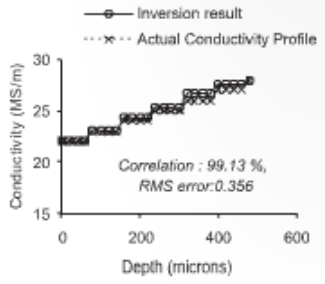

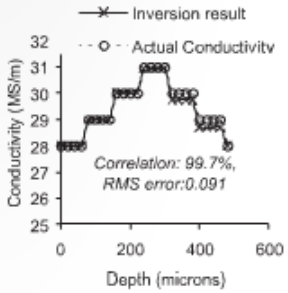

Fig. 6 : Simulated conductivity profile and the profile inverted from the "apparent" conductivity data

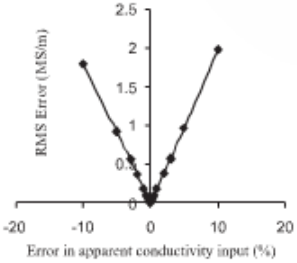

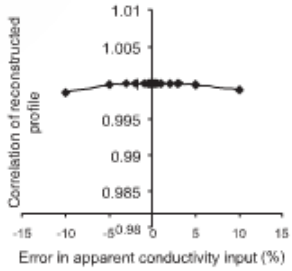

Fig. 7 : (a) RMS error in the reconstructed profile due to error in apparent conductivity input (b) Change in correlation of the reconstructed profile with the actual profile due to error in apparent conductivity input

standards at working frequencies. The success of any inversion scheme depends on its stability within this range of uncertainty.

In order to test the robustness of the proposed inversion method, linear conductivity profiles were reconstructed using "apparent" conductivities with simulated measurement errors ("noise") as input. Figure 7(a) shows the typical change in RMS error in the conductivity profile reconstructed using the proposed inversion scheme when different amounts of "noise" are added to the "apparent" conductivity inputs. Figure 7(b) shows the change in correlation of the reconstructed profile with the actual conductivity profile due to error in the "apparent" conductivity input. The "apparent" conductivity inversion scheme gives a RMS error of +0.09 MS/m or +0.3% of the substrate conductivity (s_0) for an error in "apparent" conductivity measurement of +0.5% IACS. The quality of correlation of the reconstructed profile with the actual profile is excellent even for errors as large as 10% IACS. Hence, the proposed "apparent" conductivity inversion scheme is robust enough to accommodate for reasonable measurement uncertainties.

5. INVERSION FOR SHOT PEENED SAMPLES

Fatigue cracks typically initiate from the surface since the operating stresses are often maximum at the surface. One of the most popular methods to prevent crack initiation is to induce compressive residual stresses at the surface by means of peening. In the process of shot peening, a high-velocity stream of beads are used to plastically deform the surface of a specimen. Within the plastically deformed layer, compressive residual stresses are locked in and are balanced by tensile residual stresses in the unaffected base metal. Over a uniformly peened base metal, these residual stresses are known to be axisymmetric in nature allowing analysis of "apparent" conductivity data using the proposed model.

The electrical conductivity of the cold worked layer is lower than the conductivity of the underlying base metal. Eddy current apparent conductivity measurements over a range of frequencies in most peened materials usually display a trend of decreasing "apparent" conductivity with increase in frequency (with the exception of certain alloys with piezoresistive properties). At high frequencies the depth of penetration is low and the measurement is dominated by the effect of the cold worked layer that effectively decreases the apparent conductivity. Due to large depth of penetration at lower frequencies, the effect of the cold worked layer near the surface is diminished and measured apparent conductivity approaches the substrate conductivity. On the other hand, it is well known that compressive stresses result in an increase in conductivity. The effect of cold work is predominant close to the surface and the maximum compressive stresses (thus, maximum increase in conductivities) are obtained at a certain depth below the surface. The effect of compressive stresses can be, in principle, observed by taking "apparent" conductivity measurements at multiple frequencies that would selectively reach required depths in the sample. However, the intensity of eddy currents is largely affected due to the layers of decreased conductivity close to the surface than the sub surface compressive stresses due to the skin effect. "Apparent" conductivity measurement averages out the conductivities over the depth of penetration and hence, does not reflect the true underlying conductivity profile. Further, effect of shot peening on measured "apparent" conductivity is quite modest at about 1 to 2%, making it difficult to quantify the change due to compressive stresses. However, it would be interesting to observe the trends in the actual conductivity profiles since the effect of cold work and compressive stresses on the conductivity at every depth inside the specimen can be quantitatively ascertained. In our previous study on water jet peened samples, the effect of cold work was found to be low and true conductivities provided trends consistent with the effect of residual stresses (Sundararaghavan and Balasubramaniam, 2004; Sundararaghavan et al., 2005). It is possible that similar trends might be observed in the profiles obtained from shot peening although we expect cold work to be far larger under solid impact. As discussed before (see Fig. 5), small changes in measured "apparent" conductivity can result from large changes in true conductivity over small depths, which can possibly provide sufficient resolution to capture the effect of compressive stresses. In addition to cold work and residual stresses, surface roughness effect (Blodgett et al., (2003)) and texture also causes a distortion to "apparent" conductivity measurements. The effect of crystallographic anisotropy (texture) on conductivity is assumed to be negligible and is not considered in the present study. Grid measurement methods for independent conductivity and lift-off measurements have been reported (Washabaugh et al., 2000) that makes the measurements insensitive to surface roughness effect. Figure 8 shows one such result of multiple frequency apparent conductivity measurement (Washabaugh et al., 2000) with grid measurement methods for Al 2024 samples shot peened to Almen intensities of 0.005, 0.012, and 0.017, Scale A.

In these "apparent" conductivity measurements, the unpeened sample conductivity was essentially constant with frequency which validates the quality of the reference specimen and provides the value of conductivity of the unaffected substrate (17.407 MS/m). The data shows a clear trend of decreasing conductivity with frequency, displaying the predominant effect of cold working. True conductivity profiles up to a depth of 0.384 mm were obtained from this data set by inverting the "apparent" conductivity measurements at four frequencies of 2 MHz, 1 MHz, 0.6 MHz and 0.4 MHz. These frequencies correspond to optimal depths of 0.168 mm, 0.24 mm, 0.312 mm and 0.384 mm. The results are shown in Fig. 9. Since the difference in depths between successive layers is less than 0.1 mm, the assumption of constant

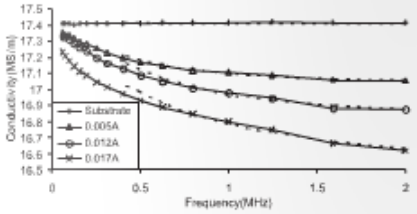

Fig. 8 : Multiple frequency measurement results for Al 2024 alloy shot peened to Almen intensities of 0.005, 0.012, and 0.017, Scale A as reported in Washabaugh et al. (2000). Dotted lines represent the apparent conductivity profiles reconstructed using specimens with conductivity profiles shown in Fig. 9.

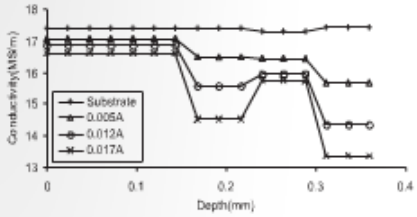

Fig. 9 : Depth profiles of conductivity reconstructed from apparent conductivity data in Fig. 8. using the proposed inversion algorithm

conductivity layers is expected to provide a good approximation. However, since "apparent" conductivity data was not provided above 2 MHz, the true profile up to a depth of 0.168 mm was not known and was approximated by a single layer of constant conductivity.

To validate the inverted conductivity profiles, apparent conductivities at 2-0.4 MHz were obtained from profiles in Fig. 9 using FEFM and are shown as dotted lines over the experimental data in Fig. 8. The results show that the reconstruction accurately represents the trend in apparent conductivity up to a frequency of 0.6 MHz (0.312 mm optimal depth). The reconstruction error becomes significant over larger depths (lower frequencies) due to the optimal skin depth approximation using the assumed substrate conductivity. For example, in the case of the high peening intensity sample (0.017 A), dotted lines in Fig. 8 show a large deviation at 0.5 MHz since the optimal depths are expected to be higher than those used in the inversion. This is because the effective conductivity of the substrate is lower than the assumed substrate conductivity due to a larger cold worked layer. On the other hand, the assumed substrate conductivity provides a good approximation for the 0.005A sample that has a smaller cold worked layer.

In all the peened samples, a large drop in conductivity is observed close to the surface up to about 0.24 mm and the drop in conductivity closely relates to the peening intensity, the largest drop occurring for the sample with highest peening intensity. This effect can be attributed to the dominant effect of cold working over the near surface layers. The trend reverses for the 0.012A and 0.017A samples, wherein a definite increase in conductivity is observed from a depth of 0.24 mm, however the conductivity is still below substrate conductivity. The effect of cold work that decreases the conductivity is possibly offset due to the opposing effect of compressive stresses causing this increase. This effect increases with increasing peening intensities as seen from the inverted profiles. Further experimental study of this effect (including measurements at significantly higher frequencies) would allow accurate characterization of conductivity profiles and possible calibration of residual stresses or the depth of maximum compressive stresses in peened specimens. Although the measurement beyond 0.312 mm carries significant reconstruction error for specimens with higher peening intensities, the trend of a drop in conductivity at depths between 0.312 and 0.384 mm is consistent for all the peened samples. This might be due to the effects of both tensile stresses in the substrate as well as the plastic strains that might exist at these depths. It is interesting to note that significant changes in the true conductivity profiles are obtained even though percentage change in the apparent conductivities at these frequencies are small, which might provide the resolution required to capture the effect of residual stresses on conductivity.

6. CONCLUSION

Motivation of this work was a study of the use of "apparent" conductivity as a basis for characterizing surface-treated specimens from processes like peening, heat treatment, cladding, coating etc. Simulations show that the "apparent" conductivity does not follow the trends followed by the actual conductivity profiles. Also, for large changes in the actual conductivity with depth, the "apparent" conductivity measurements show relatively poor sensitivities. Hence, there is a need to further process the measured "apparent" conductivity in order to obtain the information-rich conductivity gradients. A new "apparent" conductivity inversion methodology has been presented in this paper as an extension to the multi-frequency inductance inversion methodology proposed by the same authors (Sundararaghavan and Balasubramaniam, 2004). The method is specific to planar layered geometries, is computationally efficient and is applicable for online testing. A study of sensitivity of the technique indicates that the scheme is robust over a range of measurement uncertainties. An advantage that this methodology enjoys is that it does not require extensive probe calibration or design and can be used along with any commercial sensor or conductivity meters that can work over a range of

frequencies. Inversion of "apparent" conductivity measurements of shot peened samples show large changes in conductivities near the surface even though the changes in "apparent" conductivities are quite modest. A decrease in conductivity due to cold working is possibly offset due to the effect of compressive stresses at particular depths and the trend is stronger with increasing peening intensities. This interesting observation might allow possible characterization of residual stresses from peening.

Dependence on substrate conductivity for calculating the optimal depth of penetration of eddy currents leads to erroneous calculation of optimal depths in applications where large changes in conductivities are observed over the depth of the specimen. Hence, the reconstruction error progressively increases with decreasing frequencies used in reconstruction. Future work in this area involves improvement of the inverse model by using an iterative framework to eliminate the need for using optimal skin depth approximation based on substrate conductivity. This would allow accurate inversion over a larger range of frequencies. Further experimental work needs to be carried out to test the applicability of the technique for monitoring residual stresses over peened specimens.

REFERENCES

1. American Society for Nondestructive Testing, "Electromagnetic Testing" Nondestructive Testing Handbook, Vol. 5, Udpa, S.S. and P.O. Moore, eds., Columbus, Ohio, ASNT, 2004.
2. ASTM International, ASTM E 1004-99, Standard Practice for Determining Electrical Conductivity Using the Electromagnetic (Eddy-Current) Method, West Conshohocken, Pennsylvania, ASTM International, 1999.
3. Blodgett, M.P., C.V. Ukpabi, and P.B. Nagy, Surface Roughness Influence on Eddy Current Electrical Conductivity Measurements, Materials Evaluation, Vol. 61, 2003, pp.766-772.
4. Bowler, J.R. and S.J. Norton, "Theory of eddy current inversion," Journal of Applied Physics, Vol. 73, No. 2, 1993, pp. 501-512.
5. Dodd, C.V. and W.E. Deeds, "Analytical solutions to eddy-current probe-coil problems" Journal of Applied Physics, Vol. 39, No. 6, 1968, pp. 2829-2838.
6. Glorieux, C., J. Moulder, J. Basart and J. Thoen, "The determination of electrical conductivity profiles using neural network inversion of multi-frequency eddy-current data," Journal of Physics D: Applied Physics, Vol. 32, 1999, pp. 616-622.
7. Katragadda, G., J. Wallace, J. Lee, and S. Nair, "Neural network inversion for thickness measurements and conductivity profiling," Review of Progress in Quantitative Nondestructive Evaluation, Vol. 16A, D.O. Thompson and D.E. Chimenti, eds., Melville, AIP, July 1997, pp. 781-788.
8. Lavrentyev, A.I., P.A. Stuky and W.A. Veronesi, "Feasibility of Ultrasonic and Eddy Current Methods for Measurement of Residual Stress in Shot Peened Metals," Review of Progress in Quantitative Nondestructive Evaluation, Vol. 19B, D.O. Thompson and D.E. Chimenti, eds., Melville, AIP, July 2000, pp. 1621-1628.
9. Liu, G., Y. Li, Y. Sun, P. Sacks, and S. Udpa, "An iterative algorithm for eddy current inversion," Review of Progress in Quantitative Nondestructive Evaluation, Vol. 19A, D.O. Thompson and D.E. Chimenti, eds., Melville, AIP, July 2000, pp. 497-504.
10. Liu G.R. and X. Han, Computational Inverse Techniques in Nondestructive Evaluation, Boca Raton, CRC Press 2003.
11. Moulder, J.C., E. Uzal and J. H. Rose, "Thickness and conductivity of metallic layers from eddy current measurements," Review of Scientific Instrument., Vol. 63, No. 6, 1992, pp. 3455-3465.
12. Palanisamy, R. "Finite element modeling of eddy current non-destructive testing phenomena," PhD. Thesis, 1980, Colorado State University, Fort Collins, U.S.A.
13. Rekanos, I.T., T.P. Theodoulidis, S.M. Panas, T.D. Tsiboukis, "Impedance inversion in eddy current testing of layered planar structures via neural networks," NDT&E International, Vol. 30, No. 2, 1997, pp.69-74.
14. Sun, H., J.R. Bowler, N. Bowler and M.J. Johnson, "Eddy current measurements on case hardened steel," Review of Progress in Quantitative Nondestructive Evaluation, Vol. 21B, D.O. Thompson and D.E. Chimenti, eds., Melville, AIP, 2002, pp. 1561-1568.
15. Sundararaghavan, V., K. Balasubramaniam and N.R. Babu, "A multi-frequency eddy current inversion method for characterizing water jet peened aluminum alloys," Review of Progress in Quantitative Nondestructive Evaluation, Vol. 23A, D.O. Thompson and D.E. Chimenti, eds., Melville, AIP, 2004, pp. 651-658.
16. Sundararaghavan, V., K. Balasubramaniam, N.R. Babu and N. Rajesh, "A Multi-Frequency Eddy Current Inversion Method for Characterizing Conductivity Gradients on Water Jet Peened Components," to appear in Int. J. of NDT&E, 2005.
17. Uzal, E., J.C. Moulder, S. Mitra and J.H. Rose, "Impedance of coils over layered metals with continuously variable conductivity and permeability: Theory and experiment", Journal of Applied Physics, Vol. 74, No. 3, 1993, pp. 2076-2089.
18. Washabaugh, A., V. Zilberstein, D. Schlicker and N. Goldfine, "Absolute Electrical Property Measurements Using Conformable MWM Eddy-Current Sensors for Quantitative Materials Characterization," In: Proceedings of ROMA 2000 - 15th World Conference on Non Destructive Testing (WCNDT), Roma, Italy. AIPnD, 2000 (http://www.ndt.net/article/wcndt00/).

Ultrasonic Non-Destructive Evaluation (NDE) based internal inspection of pressure vessels for better maintenance practice

S.K.Nath[1] and B.H.Narayana[1]

[1] Central Power Research Institute, Thermal Research Centre, Nagpur-441 111, Maharastra, India

E-mail address: sknath2000@yahoo.com

ABSTRACT

This paper discusses about the possibility of detection of entrapped foreign object in a pressure vessel by ultrasonic inspection technique. The inspection plan is designed and illustrated here. Successful in-situ implementation of this technique will help in achieving better maintenance practice for the plant components.

INTRODUCTION

Availability of any subsystem in a thermal power plant plays a very important role in uninterrupted generation of electricity. The plant consists of number of units based on the total generating capacity. The typical capacity of one such unit may be from 110 MW to 660 MW. The steam generator of a unit of a power plant namely the boiler is one such important subsystem. A typical boiler consists of various pressure vessels e.g. headers, drums meant for containing the working fluids namely water and steam of varying temperature and pressure in the circuit. Frequent forced outages reduce its availability. One of the major causes of forced outages of the boiler is the entrapment of foreign objects inside such closed pressure vessels i.e. headers. The objects could be anything like welding rods, iron files, insulation materials, wooden pieces etc. These unwanted foreign objects restrict the flow of the working fluid causing starvation in the tubes which eventually leads to leakage. Detail failure investigation of such tubes confirms the presence of foreign objects inside the headers. Thus detection and retrieval of the foreign objects in the vessel is of prime importance to reduce the forced outages of the boiler causing huge generation loss.

Generally fibroscopic inspection is carried out for detecting the entrapped foreign material inside the headers. Inspection nipples or stub joints are cut for creating the opening for inserting the fibre-optic probe inside the otherwise inaccessible location of the headers. The inspection will detect the foreign material if it is physically present inside; otherwise no such detection will be made. However, irrespective of the detection or not, the openings created for this inspection need to be closed before restart of the plant. This requires re-welding of the cut portion, stress relieving based on thickness and radiography to check the weld quality. In case of absence of any foreign material, these are additional work serving no meaningful purposes and the same can be avoided if the information that "no foreign material is inside the header" is known by some other means. Thus a priori information regarding the presence or absence of the foreign material will help in optimizing the cutting, welding, radiography work.

An ultrasonic inspection plan is developed in the present investigation which will provide a priori information regarding the presence or absence of the foreign material inside the headers. The inspection will help in better maintenance planning with respect to optimum utilization of time and resource of plants and industries.

Inspection plan

A schematic diagram of the inspection plan is illustrated in Figure 1 below.

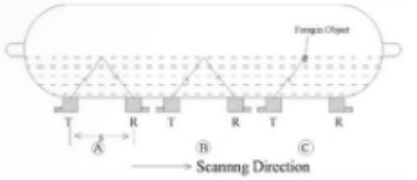

Fig. 1 : Schematic diagram of longitudinal inspection plan

The pressure vessel containing an unwanted foreign object is partially filled with stagnant water. The object could either be in suspension in water or resting in the bottom portion of the vessel depending on its specific gravity. Two ultrasonic probes; one transmitter and another receiver are placed on the surface of the vessel in a pitch-catch arrangement and scanning is performed along the longitudinal direction as in ultrasonic Time of Flight Diffraction (TOFD) inspection. However, in TOFD, the diffracted beam from the flaw is considered for its detection and sizing. Here in this case we are using the